Science of the Total Environment 745 (2020) 140924

Contents lists available at ScienceDirect

Science of the Total Environment

journal homepage: www.elsevier.com/locate/scitotenv

Chemical characterization of $PM_{2.5}$ and source apportionment of organic aerosol in New Delhi, India

Anna Tobler [a], Deepika Bhattu [a,1], Francesco Canonaco [a,2], Vipul Lalchandani [b], Ashutosh Shukla [b], Navaneeth M. Thamban [b], Suneeti Mishra [b], Atul K. Srivastava [c], Deewan S. Bisht [c], Suresh Tiwari [c], Surender Singh [d], Griša Močnik [e,f], Urs Baltensperger [a], Sachchida N. Tripathi [b,*], Jay G. Slowik [a], André S.H. Prévôt [a,*]

[a] Laboratory of Atmospheric Chemistry, Paul Scherrer Institute, 5232 Villigen PSI, Switzerland
[b] Department of Civil Engineering, Indian Institute of Technology Kanpur, India
[c] Indian Institute of Tropical Meteorology, Ministry of Earth Sciences, New Delhi, India
[d] Department of Agricultural Meteorology, CCS HAU, Hisar, Haryana, India
[e] Condensed Matter Physics Department, Jožef Stefan Institute, Ljubljana, Slovenia
[f] Center for Atmospheric Research, University of Nova Gorica, Ajdovščina, Slovenia

HIGHLIGHTS

- Over 65% of the daily $PM_{2.5}$ concentrations exceed the national air quality standard.
- Exceptionally high chloride contribution during early mornings in the cold period
- Significant solid fuel combustion contribution throughout the full campaign
- PMF uncertainty assessment

GRAPHICAL ABSTRACT

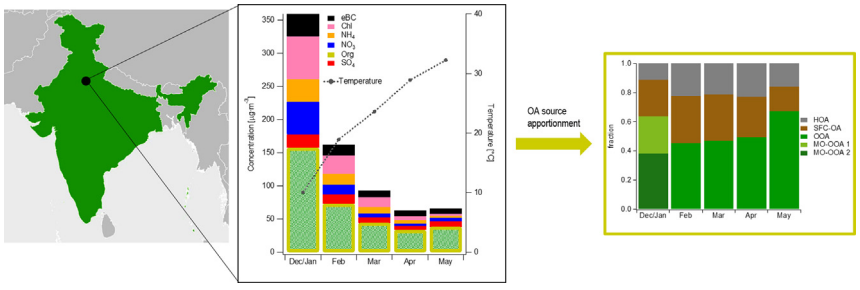

ARTICLE INFO

Article history:
Received 27 March 2020
Received in revised form 7 July 2020
Accepted 10 July 2020
Available online 13 July 2020

Editor: Pavlos Kassomenos

Keywords:
New Delhi
$PM_{2.5}$
Source apportionment
PMF

ABSTRACT

Delhi is one of the most polluted cities worldwide and a comprehensive understanding and deeper insight into the air pollution and its sources is of high importance. We report 5 months of highly time-resolved measurements of non-refractory $PM_{2.5}$ and black carbon (BC). Additionally, source apportionment based on positive matrix factorization (PMF) of the organic aerosol (OA) fraction is presented. The highest pollution levels are observed during winter in December/January. During that time, also uniquely high chloride concentrations are measured, which are sometimes even the most dominant NR-species in the morning hours. With increasing temperature, the total $PM_{2.5}$ concentration decreases steadily, whereas the chloride concentrations decrease sharply. The concentrations measured in May are roughly 6 times lower than in December/January. PMF analysis resolves two primary factors, namely hydrocarbon-like (traffic-related) OA (HOA) and solid fuel combustion OA (SFC-OA), and one or two secondary factors depending on the season. The uncertainties of the PMF analysis are assessed by combining the random *a*-value approach and the bootstrap resampling technique of the PMF input. The uncertainties for the resolved factors range from ±18% to ±19% for HOA, ±7% to ±19% for SFC-OA and ±6 % to ±11% for the OOAs. The average correlation of HOA with equivalent black carbon from traffic (eBC_{tr}) is $R^2 = 0.40$, while SFC-OA has a correlation of $R^2 = 0.78$ with equivalent black carbon from solid fuel combustion (eBC_{sf}). Anthracene (*m/z* 178) and pyrene (*m/z* 202) (PAHs) are mostly explained by SFC-OA and

* Corresponding authors.
E-mail addresses: snt@iitk.ac.in (S.N. Tripathi), andre.prevot@psi.ch (A.S.H. Prévôt).
[1] Now at: Department of Civil and Infrastructure Engineering, Indian Institute of Technology Jodhpur, Jodhpur, India.
[2] Now at: Datalystica Ltd., Park innovAARE, 5234 Villigen, Switzerland.

https://doi.org/10.1016/j.scitotenv.2020.140924

follow its diurnal trend ($R^2 = 0.98$ and $R^2 = 0.97$). The secondary oxygenated aerosols are dominant during daytime. The average contribution during the afternoon hours (1 pm–5 pm) is 59% to the total OA mass, with contributions up to 96% in May. In contrast, the primary sources are more important during nighttime: the mean nightly contribution (22 pm–3 am) to the total OA mass is 48%, with contributions up to 88% during some episodes in April.

1. Introduction

Atmospheric aerosols are recognized to have an impact on climate, visibility and human health (Fuzzi et al., 2015). Therefore, the identification and source apportionment of those particles is of great importance. Particulate matter with an aerodynamic diameter smaller than 2.5 μm ($PM_{2.5}$) has been widely used as a proxy for air pollution, for example in the WHO Air Quality Guidelines (WHO, 2005), which are used worldwide as a reference. In case of $PM_{2.5}$, a daily average of <25 μg m^{-3} with an annual mean average of 10 μg m^{-3} should be targeted. Most megacities experience problems reaching these targets. In the past few years, New Delhi, India, has always been ranked in the top most polluted cities in the world (IEA, 2016). During special occasions, like the Diwali fireworks in November, high levels of up to 1200 μg m^{-3} can be observed in New Delhi (Tiwari et al., 2012). As long-term exposure to high ambient $PM_{2.5}$ concentrations is linked to cardiovascular disease and premature death (Pope and Dockery, 2006), the emission sources have to be better understood in order to be targeted specifically and to efficiently reduce the high pollution levels.

Previous aerosol studies in New Delhi have mostly focused on offline analysis of total PM concentrations (Tiwari et al., 2012), trace elements (Kumar et al., 2018; Pant et al., 2016) or black carbon measurements (Tiwari et al., 2013). They identified traffic, residential and industrial combustion and open fires, including waste burning as the most important anthropogenic emission sources in the city. It was estimated that open municipal solid waste burning may contribute up to 5–11% to the total PM emitted within Delhi (Nagpure et al., 2015). In addition to the local urban air pollution sources, New Delhi is affected by regional air pollution sources from the Indo-Gangetic Plain, often dominated by open outdoor fires from agricultural regions. It is common practice in Northern India to clear field crops by burning the residual stubbles. These fires are common in April to May (pre-monsoon) and even more in October to November (post-monsoon) (Liu et al., 2018).

The main limitations of previous studies are either low temporal resolution (with typically daily samples) or short campaign periods. With our measurements we present 5 months of measurements with high time resolution of ambient $PM_{2.5}$. The aerosol chemical speciation monitor (ACSM) is a robust mass spectrometer, especially designed for long-term measurements. It is widely used by research groups and monitoring networks all over the world (Petit et al., 2015; Zhou et al., 2019; Budisulistiorini et al., 2014; Fröhlich et al., 2015b). Co-located instruments showed a good inter-comparability (Crenn et al., 2015; Freney et al., 2019), and it is well suited for organic aerosol source apportionment (Fröhlich et al., 2015a).

Recently, the use of online aerosol mass spectrometry for PM source apportionment has been reported in New Delhi. Gani et al. (2019) reported the first long-term measurements of non-refractory (NR) submicron PM (PM_1) levels and their strong dependence on meteorology. Subsequently, Bhandari et al. (2019) presented a source apportionment of the same data set. Our measurements have the advantage to report the more relevant $PM_{2.5}$ levels regarding legal thresholds. In addition, we are able to access more molecular information because of a wider mass range measured. In combination with advanced source apportionment techniques it allows to better understand the emission sources in Delhi.

In this study, we present a detailed characterization of the chemical composition of $PM_{2.5}$ in New Delhi combined with source apportionment based on positive matrix factorization (PMF) (Paatero and Tapper, 1994) analysis of the organic mass spectra measured by a time-of-flight aerosol chemical speciation monitor (ToF-ACSM) (Fröhlich et al., 2013). This will improve the current understanding of the PM pollution in New Delhi and of the source of carbonaceous aerosols which are important regarding health and climate forcing of particles. Finally, this work may support mitigation strategies in and around New Delhi towards green chemistry.

2. Method

2.1. Sampling site and instrumentation

To investigate the $PM_{2.5}$ concentration and composition evolution in New Delhi with high time resolution, a ToF-ACSM (time of flight aerosol chemical speciation monitor, Aerodyne Research Inc., Billerica, MA, USA) (Fröhlich et al., 2013) and a seven-wavelength aethalometer model AE33 (Magee Scientific, Berkeley, CA, USA) (Drinovec et al., 2015) were installed at the Indian Institute of Tropical Meteorology (IITM, 28°35′ N; 77°12′ E) in New Delhi (India). The institute is located north of the Central Ridge reserve forest in a residential area of New Delhi.

Ambient aerosols were sampled continuously at a flow rate of 5 L min^{-1} through stainless steel tubing. The inlet was equipped with a $PM_{2.5}$ cyclone (BGI, Mesa Labs, Inc.) and installed on the rooftop of the building. The ambient aerosol then entered the temperature-controlled room in the floor below. Before passing through a Nafion dryer (MD-110-48S-4), a by-pass flow of 1.9 L min^{-1} was installed to maintain a constant total flow required for the cyclone. After the Nafion dryer the flow was split, so that 0.1 L min^{-1} were sampled by the ACSM and 3 L min^{-1} by the aethalometer. The 3 L min^{-1} are needed for near-isokinetic sampling conditions at the ACSM (Aerodyne Research Inc. and Tofwerk AG, 2019).

2.1.1. Aerosol chemical speciation monitor (ACSM)

The ToF-ACSM provides quantitative mass spectra of the non-refractory component of $PM_{2.5}$. Its operating principles are described in detail in the literature (Fröhlich et al., 2013) and summarized here. Particles first pass through a 100 μm critical orifice and are then focused into a narrow beam by an aerodynamic lens. In order to sample $PM_{2.5}$ particles, the ACSM was equipped with an intermediate pressure lens (IPL) as described in Xu et al. (2017). The non-refractory fraction of the focused particle beam is then flash-vaporized in a standard tungsten vaporizer at ~600 °C. The vaporized compounds are ionized by an electron impact (EI) ionization source (70 eV) and analyzed with a time-of-flight (ToF) mass spectrometer. The ACSM alternates between direct sampling from ambient air and through a particle filter inserted into the sampled airflow; the difference of these two measurements yields the ambient mass spectrum. The obtained mass spectra had a mass to charge (m/z) range of 12–210 Da with a resolution of $m/\Delta m = 120$ at m/z 28. This does not allow a separation of different ions at the same integer m/z. Consequently, all signal is integrated on an integer-by-integer basis. Mass calibration was performed by generating mono-disperse

300 nm particles of ammonium nitrate and ammonium sulfate by injecting them into the ACSM and a condensation particle counter (CPC, TSI model 3776, Shoreview, MN, USA) (Ng et al., 2011).

Two different filter switching schemes were used during the measurement period. From 22 December 2017 until 17 January 2018, the ACSM alternated between 2 min of filtered air and 8 min of ambient air ("slow valve switching settings"). From 17 February 2018 until 26 May 2018, the ACSM sampling system switched every 20 s between filtered and ambient air ("fast valve switching settings"). Regardless of switching scheme, spectra were integrated over a 10 min period (i.e. 1 cycle for the slow settings and 15 cycles for the fast settings), resulting also in a time resolution of 10 min. The ion source filament was changed on 6 May 2018.

The raw data were separately analyzed for the two measurement settings by using Tofware 2.5.13. For the slow valve switching settings, an experimentally determined relative ionization efficiency for ammonium (RIE_{NH4}) of 3.33 and for sulfate (RIE_{SO4}) of 2.27 was used, while for chloride (RIE_{Chl}) and organics (RIE_{Org}) a standard RIE of 1.4 was assumed. For the fast valve switching settings, an $RIE_{NH4} = 2.83$ and $RIE_{SO4} = 1.06$ were applied before 6 May 2018 and $RIE_{NH4} = 4.18$ and $RIE_{SO4} = 0.92$ for the new filament after 6 May. Based on the NH_4NO_3 calibrations, a mean inorganic salt interference on CO_2 (Pieber et al., 2016) of 7% was subtracted from the organic m/z 44 signal for the data measured with the slow valve switching settings (December/January) and 1.7% for the measurements with the fast valve switching settings (February–May). The collection efficiency was evaluated according to the method of Middlebrook et al. (2012). We observed no sufficiently acidic particles to influence the calculations and the NH_4NO_3 mass fraction was <0.4 in >99% of the measurements during the whole campaign. Therefore, a collection efficiency (CE) of 0.5 was assumed.

2.1.2. Aethalometer

The Magee Scientific Aethalometer model AE33 collects ambient particles on a filter tape and continuously measures the light attenuation at seven wavelengths (370, 470, 520, 590, 660, 880 and 950 nm) with 1 min time resolution. With the dual-spot technique in the AE33, the instrument is able to correct loading non-linearities in real-time (Drinovec et al., 2015; Drinovec et al., 2017). These light attenuation measurements were converted to equivalent black carbon (eBC) concentrations using the nominal mass absorption cross section (MAC) value of 7.77 $m^2\ g^{-1}$ for the measurement at 880 nm. During the measurement campaign, three different filter tape types were used: PALL Flex TFE coated FiberFilm T60 (M8020; described in Drinovec et al. (2015)), M8050 and M8060. Although the AE33 is able to correct loading effects in real-time, the correction, especially for the M8050 tape, is not always sufficient, mainly due to high mass loadings and non-linearities exceeding the real-time capabilities of the instrument. Therefore, we manually corrected the data by fitting the slope to the BC(ATN) (BC as a function of attenuation) plot (Drinovec et al., 2015). Overall, the uncertainty on the correction slope is about 5%.

2.2. Source apportionment

2.2.1. OA source apportionment

The ToF-ACSM data was averaged to 30 min. Positive matrix factorization (PMF) (Paatero, 1997; Paatero and Tapper, 1994) was applied on the organic mass spectra measured by the ToF-ACSM. PMF is a bilinear receptor model with non-negativity constraints. It describes the variability of a multivariate data set **X**, here a sequence of organic mass spectra, as a linear combination of factor contributions (time series) **G** and factor profiles **F**. The residual matrix **E** contains that fraction that could not be described by **G** and **F** and is defined by Eq. (1):

$$X = GF + E \tag{1}$$

The dimensions of **G** and **F** are depending on the rank p, which represents the number of factors chosen to describe the data set. In order to solve Eq. (1), the quantity Q (Eq. (2)), defined by the elements of the residual matrix **E** (e_{ij}) and the measurement uncertainty (σ_{ij}), is minimized:

$$Q = \sum_{i=1}^{n}\sum_{j=1}^{m}\left(\frac{e_{ij}}{\sigma_{ij}}\right)^2 \tag{2}$$

PMF suffers from rotational ambiguity, i.e. there exist rotated solutions of **G** and **F** with similar Q-values, out of which some may result in environmentally unreasonable solutions and/or mixing of factors. It has been demonstrated that constraining expected factor profiles is an efficient method for rotational exploration to optimize the factor deconvolution (Crippa et al., 2014; Canonaco et al., 2013; Fröhlich et al., 2015a). For the following analysis, PMF was implemented within the multilinear engine (ME-2) (Paatero, 1999), using Source Finder (SoFi, Datalystica Ltd., Villigen, Switzerland) (Canonaco et al., 2013) for model configuration and post-analysis. The SoFi/ME-2 package allows the use of a priori information in the PMF analysis, so that elements of either the **G** and/or **F** matrix can be constrained from known factor profiles and/or factor time series. Factor profiles can either be from ambient measurements where a clear separation of the sources was successful or from chamber experiments. The extent to which the profiles or times series are allowed to deviate from the predefined values is determined by the so-called a-value (Eq. (3)):

$$f_{j,solution} = f_j \pm a \cdot f_j \tag{3}$$

where f represents the constrained factor profile in the **F** matrix.

To estimate the rotational and statistical uncertainty of the solution, a random a-value approach combined with bootstrap resampling analysis (Davison and Hinkley, 1997) was performed. During each iteration step of the bootstrap analysis, random samples of the original data and error matrix were selected to create new input matrices that have the same dimensions as the original input matrices. Then, PMF with a random a-value was performed. A random a-value ranging between 0 and 0.5 to account for the adaption of the constrained profile was separately assigned to each constrained factor for each bootstrap iteration. The large number of PMF solutions was assessed by application of a selection of criteria based on typical profile or time series features for the different factors. The set of applied criteria is described in details in Section 3.2. Based on those criteria, environmentally unreasonable solutions were rejected. The rotational and statistical uncertainty of the averaged PMF solution can be assessed since multiple solutions exist for different time points i exist due to the random resampling (bootstrapping) and the random a-value for constrained factors. This uncertainty is described by the linear fit through zero between the standard deviation for each point versus the mean of that time point in the averaged PMF solution. The reported uncertainty (in percentage) for each factor is given by the slope of the linear fit described beforehand and will not include other errors such as the model uncertainty (e.g. number of factors chosen).

2.2.2. eBC source apportionment

Light absorbing aerosol from wood burning, including black carbon from this source (eBC_{wb}), has a significantly stronger absorbance in the ultraviolet (UV) and lower visible range compared to black carbon from traffic contributions (eBC_{tr}). Based on this observation, Sandradewi et al. (2008) devised a model for the separation of biomass burning and traffic contributions to eBC using the multi-wavelength aethalometer measurements. Zotter et al. (2017) proposed Ångström exponents of 0.9 and 1.68 for traffic and wood burning, respectively, based on comparison with ^{14}C elemental carbon (EC) measurements. This method has been successfully applied in places where no other major combustion sources were present.

The absorption Ångström exponent (AAE) is calculated based on the absorption coefficients b at 470 nm and 950 nm (Eq. (4)):

$$AAE = \frac{\ln\left(\frac{b_{470\ nm}}{b_{950\ nm}}\right)}{\ln\left(\frac{950}{470}\right)} \quad (4)$$

The AAE frequency distribution from the measurements in New Delhi is centered on 1.2 and suggests an AAE_{tr} value of 0.9 for traffic (like Zotter et al. (2017)) and an AAE_{sf} value of 1.5 for solid fuel combustion. The latter value is a rough estimate based on the pdf (probability density function) of the AAE values (Fig. S1) and is somewhat lower than the one found by Zotter et al. (2017) for wood burning. We expect a wide range of different open burning sources in addition to biomass burning in Delhi, therefore we chose to call this type of combustion "solid fuel combustion" (resulting in eBC_{sf}). The optical properties and absorption wavelength dependency of eBC and other carbonaceous aerosol from sources other than wood combustion such as coal combustion or waste incineration are unknown and/or poorly characterized. In addition to the uncertain chemical composition of the coating, this coating and the non-refractory carbonaceous aerosol core can also be altered by bleaching: Zhao et al. (2015) showed that in highly oxidizing atmospheres, the brown carbon (BrC) can be severely bleached, leading to an underestimation of eBC_{sf} in the source apportionment.

3. Results and discussion

3.1. $PM_{2.5}$ chemical composition

Fig. 1 shows the temporal variation (in India Standard Time (IST)) of the NR-$PM_{2.5}$ organics, chloride, nitrate, ammonium, and sulfate, as well as the relative contributions of these species to the total NR- $PM_{2.5}$ mass loadings, and the eBC concentration. The period highlighted in blue was recorded using the slow valve switching parameters, the period highlighted in yellow was measured with the fast valve switching settings. The highest pollutant concentrations are found during the colder period between December and February. The hourly total NR-$PM_{2.5}$ concentration varies from 10 to over 600 μg m^{-3}, whereas >65% of the daily averaged data exceed the 24 h air quality standard of 60 μg m^{-3} defined by the Central Pollution Control Board, India. The hourly eBC mass loadings range from 1 μg m^{-3} in the afternoons during May up to 120 μg m^{-3} during December and January nights.

The total $PM_{2.5}$ concentration shows a distinct seasonal and diurnal variation. During December/January, an average mass concentrations of 359 μg m^{-3} is measured, strongly driven by the high loadings measured during the nights. With the increase of the average temperature and the correspondingly greater planetary boundary layer (PBL) height, the monthly average mass concentration decreases during the transition from winter to spring. The mean average mass loading in May is 65.6 μg m^{-3}, roughly 6 times lower compared to December/January (Fig. 2). The organics are the dominant species in all months, representing 44% in December/January and 58% in May of the total $PM_{2.5}$ mass. The strongest seasonal change in absolute mass loading and relative contribution is observed for chloride. During December/January, peak concentrations above 200 μg m^{-3} are observed, including some events where chloride concentrations are higher than any other species measured by the ACSM. In May, the monthly averaged relative contribution is 4 times lower than in the winter months, whereas the absolute concentration is 25 times lower. This is comparable with the PM_1 measurements conducted by Gani et al. (2019) where they observed a similarly drastic decrease of the unusual high chloride concentrations. The ammonium chloride that is observed during winter is expected to evaporate with the high temperatures and low relative humidity in summer and then to be found in the gas phase (primarily as HCl) rather than the particle phase.

Besides the seasonal variations in the $PM_{2.5}$ concentration and contribution of the ACSM species and BC to the total mass, a pronounced diurnal pattern (Fig. S2) is observed as a result of surface meteorology, PBL dynamics and source emissions. A similar trend for the composition based estimate for PM_1 (C-PM_1 = BC + NR-PM_1) concentrations at the Indian Institute of Technology Delhi was observed by Gani et al. (2019).

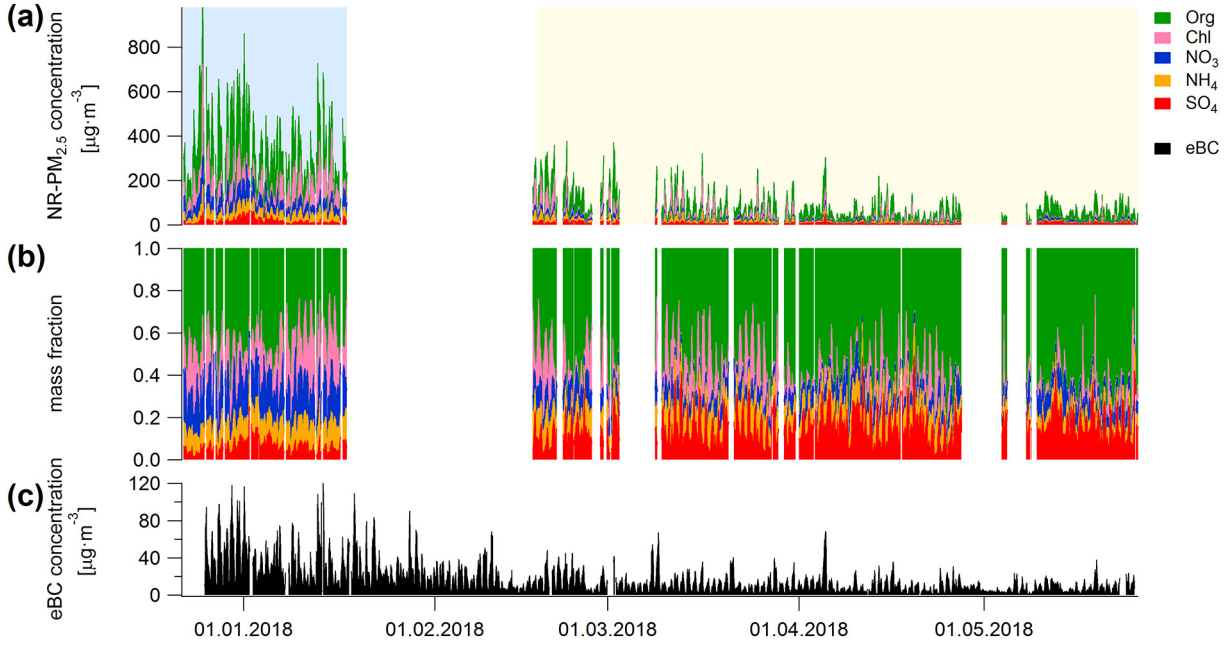

Fig. 1. (a) Absolute stacked concentrations of hourly non-refractory organic (green), chloride (pink), nitrate (blue), ammonium (orange) and sulfate (red) measured by the ToF-ACSM in the slow (light blue) and fast (light yellow) valve switching mode and (b) relative contributions of the species to the total NR-$PM_{2.5}$ aerosol concentration. (c) Time series of equivalent black carbon measured by an aethalometer AE33. (For interpretation of the references to colour in this figure legend, the reader is referred to the web version of this article.)

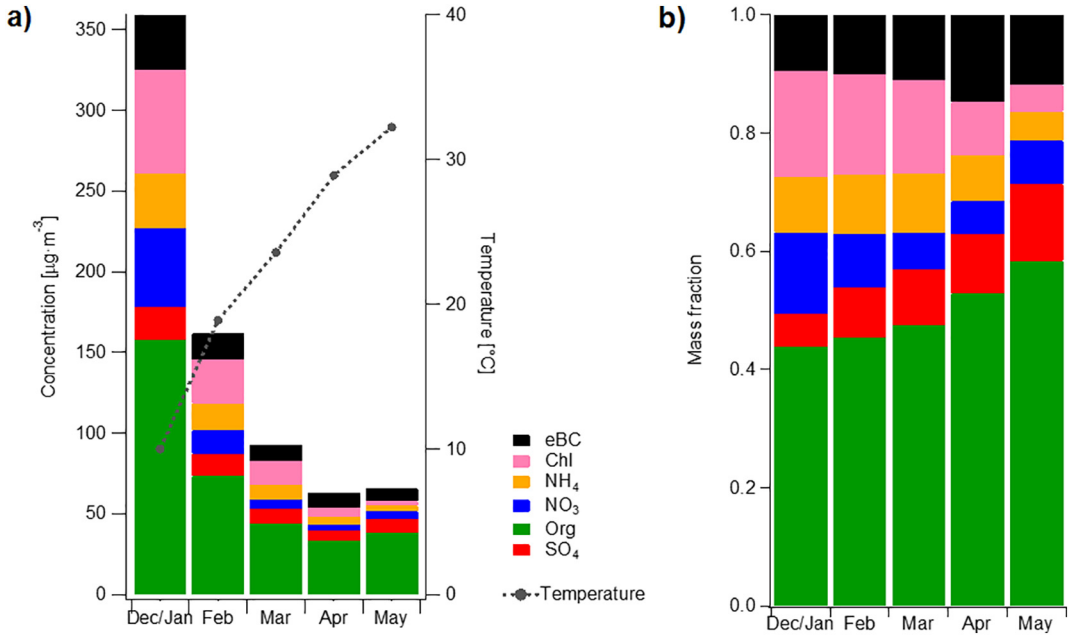

Fig. 2. (a) Average chemical composition and concentration of total PM2.5 at IITM and temperature (from the DPCC station at Mandir Marg, roughly 2.7 km air distance) and (b) relative contributions of the species to the total mass per month.

3.2. OA source apportionment

During this campaign, two different valve switching modes were used. It has been shown, that different valve switching times can alter ACSM mass spectra, because for some compounds evaporation timescales are comparable to or longer than typical switching periods (Fröhlich et al., 2015a). These differences may be large enough so that PMF factor mass spectra are not consistent between sample periods having different valve switching times. In addition, Fröhlich et al. (2015a) showed in an intercomparison study that the f_{44} discrepancies between the instruments resulted in significant differences in the PMF factor profile analysis but not in the total factor contribution. In the scatter plot of f_{44} vs. f_{43} (fraction of m/z 44 and 43 to organic mass, respectively), a significant change is observable when the instrument valve switching settings were changed (Fig. S3). Therefore, the source apportionment for this data set was performed on the two periods separately. Furthermore, the period with the fast valve switching settings was subdivided again to account for the difference in f_{44} that resulted from changing the filament end of April.

In a first step, the number of factors was determined based on inspection of the source profiles, diurnal variations, comparison with eBC source apportionment and residual analysis. The solution best representing the total OA includes a hydrocarbon-like OA (HOA), a solid fuel combustion OA (SFC-OA) and two or one oxygenated OA (OOA) factors. In contrast to other source apportionment studies in Europe and Asia, a clean biomass burning OA (BBOA) could not be separated even though there are indications for such source emissions. In winter, BBOA is often associated with domestic heating based on wood, whereas in other seasons wildfires and agricultural burning are the dominant sources for BBOA. In April and May, agricultural burns for field clearing are important, which is also manifested in the strong increase of registered fires outside of Delhi (FIRMS, 2019). From December to February, when temperatures are still low, it can be assumed that residential heating is more dominant, with only little fire activity reported around Delhi. However, wood is often not available for low-income households, so other alternative energy sources like paper, dung, textiles, plastic and compostable waste are also burned (Nagpure et al., 2015). However, a SFC-OA factor was separated which includes probable emission sources of wood and coal combustion, agricultural waste (stubble) burning, waste disposal and open fires. A detailed description of these OA sources is described in Sections 3.2.1 and 3.2.2 for the two periods. The main difference to the PMF results published by Bhandari et al. (2019) is that with our analysis we are able to also access information from $m/z > 120$ (the limit for a quadrupole ACSM). Furthermore, using the SoFi/ME-2 package allows the constraint of factors. Therefore, we were able to separate the primary sources in more detail (i.e. the separation of HOA and SFC-OA) during the full period discussed here.

To assess the statistical and rotational uncertainty, the input data matrix was repeatedly ($n = 1000$) and randomly resampled (bootstrap strategy) and each time a random a-value for the constrained factors was chosen. This generates a large number of PMF runs that need to be examined. To identify the environmentally reasonable solutions, a set of criteria was applied. In each criterion, the factor profile or time series for each bootstrap iteration is reduced to a single point, a so-called score (Canonaco et al., 2020). A threshold for each criterion is set based on the evolution of the scores over all PMF iterations and/or the score for the base case. Only the solutions that fulfill all criteria simultaneously are kept and regarded as environmentally reasonable.

HOA optimization. In the unconstrained PMF solutions, the mass spectral profiles indicated mixing of the combustion sources. To minimize the mixing between SFC-OA and HOA, the HOA profile was constrained using the profile that was found in Paris during winter by Crippa et al. (2013b) with a random a-value between 0 and 0.5. Since the BC source apportionment is associated with large uncertainties, the correlation of HOA and eBC_{tr} was not used as a criterion to exclude solutions.

SFC-OA optimization. For December/January (slow settings), the SFC-OA was left unconstrained, whereas for the warmer period (February–May, fast settings) the SFC-OA was not clearly separated as a primary source if not constrained. For constraining the SFC-OA factor, using the SFC-OA mass spectral profile from December/January was not successful, i.e. the constrained factor did not explain much mass and/or the signal of ions typically associated with combustion processes (m/z 60, 73 and 202). In addition, a mixed primary factor with those ions was resolved. Therefore, a clean primary SFC-OA

was first separated which then could be used for constraining this factor in the later PMF analysis. Higher contributions of SFC-OA are expected in February and during the night due to an increase of residential heating. So PMF was first run for only the night hours in February to get a clean SFC-OA profile for that period. This profile was then constrained with a random a-value in the range of 0 to 0.5. To separate the environmentally reasonable solutions, the explained variation of m/z 60 was monitored. Based on the pdf (probability density function) over all PMF runs the extreme runs were discarded, which corresponds to a lower limit of an explained variation of m/z 60 of 0.59, 0.38 and 0.32 for December/January, February–April and May, respectively. The correlation with eBC_{sf} was monitored but was high ($R^2 > 0.62$) over all solutions and was therefore not used to exclude solutions.

OOA optimization. The OOA factor (or both of them) was always left unconstrained in this analysis and is characterized by a very high contribution of m/z 44. To corroborate the secondary nature of the OOA factor(s), the contribution of m/z 44 was monitored to make sure that all PMF solutions included the contribution of that ion. In December/January, two OOA factors were separated, the MO-OOA 1 factor with some aliphatic signatures, whereas those were less pronounced in the MO-OOA 2 factor. There are no unique markers specifically only relating to one of the MO-OOA factors to track. However, from analysis of single PMF runs, solutions with a low f_{44}/f_{43} in the MO-OOA 1 were typically associated with a higher f_{44} in the SFC-OA, indicating mixing of MO-OOA 1 with the SFC-OA factor. Consequently solutions with an $f_{44}/f_{43} < 1.5$ in the MO-OOA 1 factor were rejected. Apart from their difference in the mass spectral profile, the diurnal for MO-OOA 2 is unique with a distinct maximum around 10 am and high concentrations throughout the day. Therefore, the diurnal pattern was monitored, and solutions that did not have a peak in the morning at 10 am that is comparable (or higher) to the concentrations at midnight ([concentration at 10 am]/[concentration at midnight] < 0.9) were rejected. In December/January, all solutions that did not exhibit this pronounced peak in the late morning were already rejected by other criteria, whereas in February–April and May this influences the selection of solutions more. The OOA factor in the solution for February–April and May is similar to the MO-OOA 2 factor, and the MO-OOA 2 criteria were applied.

3.2.1. December/January (slow valve switching settings)

The solution that best represented all variations in this period was a 4-factor solution which includes two primary factors, HOA and SFC-OA and two oxygenated factors, MO-OOA 1 and MO-OOA 2. The MO-OOA 1 and MO-OOA 2 factor mainly differ in the contribution of aliphatic ions in the profile (higher for MO-OOA 1) and a different diurnal trend (high concentrations throughout the full day for MO-OOA 2). All the factors are discussed in detail below. In the 3-factor solution (Fig. S4), the two MO-OOAs are combined in one OOA factor with similar contribution as the sum of the two MO-OOA factors. The 5-factor solution leads to mathematical splitting of the MO-OOA 1 into an aged mixed primary OA and an OOA with a similar profile as MO-OOA 2 (small aliphatic signatures) but the diurnal of MO-OOA 1 (low concentrations during the afternoon hours). With an even higher number of factors, the OOA factors keep splitting and/or an environmentally non-explicable factor is resolved. The presented result is the average of all solutions that were accepted as environmentally reasonable based on the criteria above. The factor profiles and the diurnal concentrations together with the eBC source apportionment are shown in Fig. 3. From the initial 1000 bootstrap runs, 930 solutions match the criteria described above. Similar to the total $PM_{2.5}$ and OA concentration, the diurnals are partially driven by the PBL dynamics. During the night, a very low PBL height can be observed (Gani et al., 2019) which favors the accumulation of all emissions. Nevertheless, some distinct factor-dependent features are apparent.

The constrained HOA factor is characterized by the presence of alkyl-fragment signatures, the absence of anhydrous sugar fragments and a strong contribution of m/z 43 compared to m/z 44. The vehicle fleet in New Delhi is slightly different from the reference spectrum from Paris (Crippa et al., 2013b). In 2018, >11 million vehicles were registered in Delhi, whereof 64% were motorized two wheelers (Accident Research Cell et al., 2018). Two-wheelers only contribute 6% to the total vehicle

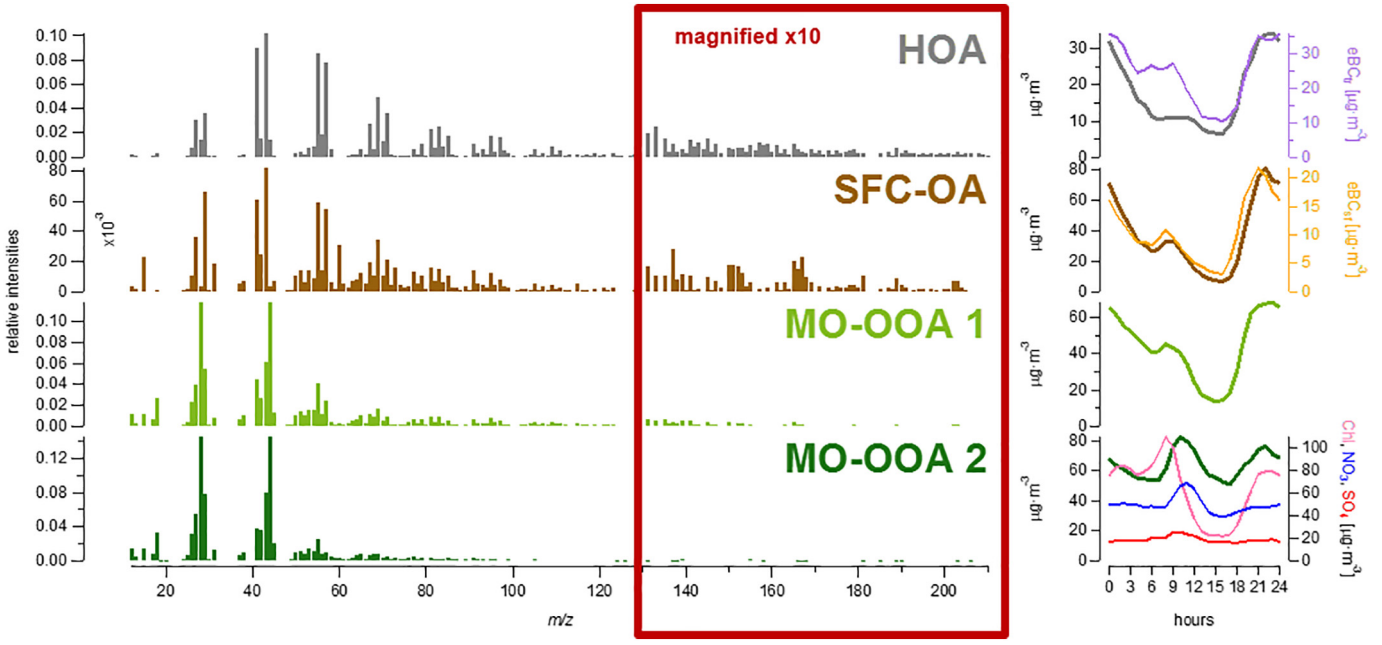

Fig. 3. Mean PMF factors mass spectra (left) and mean diurnal mass concentrations (right) for the cold period. Additionally, the diurnal profiles of eBC_{tr}, eBC_{sf} (from source apportionment of AE33 data) and chloride are shown with the corresponding ACSM factors.

fleet in France (European Commission, 2018). Although the contribution of two-wheelers in cities can be assumed to be higher than in the country-side, the fraction of two-wheelers in Paris is still significantly lower than in Delhi. The majority of passenger cars (60%) and light commercial vehicles (95%) were running on diesel in France in 2017 (CCFA, 2019). In contrast, in Delhi the majority of cars (53%) run on petrol in 2013 (Goel et al., 2016). Meanwhile, the HOA profile from Paris has been shown to perform well for a wide variety of places, seasons and car fleets (Crippa et al., 2014; Elser et al., 2016). In addition, sensitivity tests on the amount of f_{44} in the reference profile used were performed and the environmentally most reasonable solution was found with the original reference profile. The profile was constrained with an average a-value of 0.26 ± 0.14. The averaged error for the modelled HOA is calculated based on the standard deviation of all points in the time series of the accepted solutions versus the mean of the averaged solution. The uncertainty is defined as the slope of the linear fit through zero. An uncertainty of ±19% is estimated. The diurnal pattern shows a small morning rush hour peak around 9 am and elevated levels from the evening on during the night. The eBC source apportionment shows a more pronounced early morning rush hour peak, however, its source apportionment is more uncertain for the reasons described in Section 2.2.2. The median HOA/eBC_{tr} is 0.59, somewhat higher than the reported OM/BC range from 0.2 to 0.4 in smog chamber experiments (Chirico et al., 2010) but consistent with the range from 0.3 to 0.6 found in ambient measurements in Paris (Crippa et al., 2013a). Note, however, that the median HOA/eBC_{tr} increases to 1.13–1.26 during spring. Trends for higher OM/BC can be found with high organic mass loadings due to the influences on the partitioning of the organic compounds (Chirico et al., 2011) and older vehicles without diesel particle filters (Chirico et al., 2010). This is both in agreement with the higher mass loadings and older car fleet in New Delhi compared to Europe. Alternatively, it may reflect uncertainties in the determination of eBC_{tr} caused by the assumption of static AAE values for both traffic and SFC, despite seasonal changes in the SFC fuel distribution. Although local heavy-duty vehicles, auto-rickshaws and buses have been converted to CNG (Ravindra et al., 2006), regional transport still involves diesel traffic without filters. In order to control the pollution levels and traffic volume during the day, since February 2013, heavy duty vehicles have been banned from entering the city through rush hours from 7:30 to 11 am and 5 to 7 pm (Singh, 2013). Furthermore, during heavy pollution days heavy duty vehicles are often banned on short notice in the city center from 7 am to 11 pm. Considering that heavy-duty vehicles are only allowed inside the city during the night hours and the PBL dynamics, it is reasonable to have higher HOA concentrations during the night compared to the morning rush hour peak. Similar observations were made based on source apportionment of AMS data and PTR-MS data, which were measured at the Indian Institute of Technology Delhi (IITD). AMS PMF analysis resolved one HOA factor with a similar diurnal as shown by ACSM PMF (Lalchandani et al., 2020). PTR-MS PMF analysis resolved two traffic factors, both of which also show a morning rush hour peak and a broad peak during nighttime (Wang et al., 2020).

The SFC-OA shows high contribution of the mass fragments m/z 60 and m/z 73, which are related to anhydrous sugars, typical for biomass burning. It also includes signals from unsaturated hydrocarbons at m/z 77, 91 and 115, as is also the case for coal combustion (Elser et al., 2016; Dall'Osto et al., 2013). Furthermore, contributions of m/z 178 and m/z 202, associated with anthracene and pyrene, two PAHs that are typically emitted during combustion processes, are present. Therefore, we argue that this combustion factor is a mixture of different solid fuel combustions. Consistent with residential heating activities, SFC-OA exhibits a diurnal pattern with a small peak in the morning hours and a significant increase over the night. During the day, the SFC-OA is close to zero. This also agrees with the fact that SFC-OA is a primary emission source. In Delhi, solid fuel combustion may comprise a mix of domestic heating, coal-based cooking and open-fire activities which include many types of biomass burning and waste combustion. Resolution of these individual emissions sources could not be achieved using only the current ACSM measurements. The averaged uncertainty of the SFC-OA is ±7%. Even though the BC source apportionment is based on the assumption of only having two combustion sources, which seems too simple for New Delhi and its various combustion sources, the eBC_{sf} resolved with the aethalometer model correlates surprisingly well with our SFC-OA factor. Over the whole period the time series yield a correlation of $R^2 = 0.69$, with a median ratio SFC-OA to eBC_{sf} of 3.30, while the diurnal variations exhibit a correlation of $R^2 = 0.88$ in the averaged solution. The reported OM/BC values for wood combustion are highly dependent on the combustion conditions and span a wide range from 1.1 to 10 (Favez et al., 2010; Grieshop et al., 2009). This large variation is due to different measurement techniques and burning conditions. In addition, ambient measurements tend to report higher OM/BC ratios. In general, a more efficient combustion leads to lower OM/BC values. With the many open burning activities observed in New Delhi, higher OM/BC values are expected as the combustion is often not operated under ideal conditions.

During this time period we are able to distinguish two OOA factors, based on different profile contributions and diurnal variations. The uncertainty of the two OOA factors is similar, the averaged error is ±9% for MO-OOA 1 and ±8% for MO-OOA 2. Compared to the two primary factors, the MO-OOA 1 and MO-OOA 2 factors exhibit a significantly higher contribution of m/z 44, typically a result of thermal decomposition of highly oxygenated organic acids (Ng et al., 2010). Besides the high contribution of m/z 44, the MO-OOA 1 factor still shows some aliphatic features in the profile. This is also reflected in the diurnal profile where high concentrations during the night dominate. The MO-OOA 2 factor shows a different diurnal pattern with rather high concentration levels during the full day and a unique peak in the late morning hours (10 am). When the chloride concentration decreases, an increase in the MO-OOA 2 factor is noted. This may be linked to specific oxidation chemistry occurring in environments that are rich in chloride and HONO; this is the case during the late morning hours in New Delhi. The following decrease in the concentration around noon is likely due to PBL dynamics.

3.2.2. February–May (fast valve switching settings)

During the measurements with the fast valve switching settings from February until May 2018, the filament had to be replaced which resulted in an increased f_{44} with the new filament compared to the old one. Therefore separate PMF runs were performed for the two filament periods. It was found that a 3-factor solution best represents the OA variations, independent of the filament. A higher number of factors led to an additional primary factor with features of both HOA and SFC-OA but no m/z 44. An even higher number of factors led to mathematical splitting of the OOA factor. From the 1000 bootstrap runs, 977 solutions for the analysis for February to April and 979 solutions for May met the criteria described above. The averaged factor profiles and the diurnal concentrations are shown together with the eBC source apportionment in Fig. 4. Since the solutions are very similar for the two separate PMF analyses, they are discussed together in this section. The mentioned a-values, uncertainties and ratios refer to the separate studies (February–April and May, respectively).

An HOA factor similar to the solution in December/January with the slow valve switching settings was resolved, with the same key features. The diurnal pattern was the same, with a small rush-hour peak in the morning and high concentrations during the night due to heavy-duty traffic that is only allowed in the city between 11 pm and 7 am. A mean a-value of 0.25 ± 0.15 for both solutions was found, with an uncertainty of the HOA factor of ±19% and ±18%, respectively. As mentioned in Section 3.2.1, the median HOA/eBC_{tr} is 1.13 and 1.26, respectively. Further discussion follows in Section 3.2.3.

The SFC-OA contribution is expected to be lower in the warmer months with temperatures up to 36 °C in April compared to the still relatively cold month of February. In addition, the high temperatures can

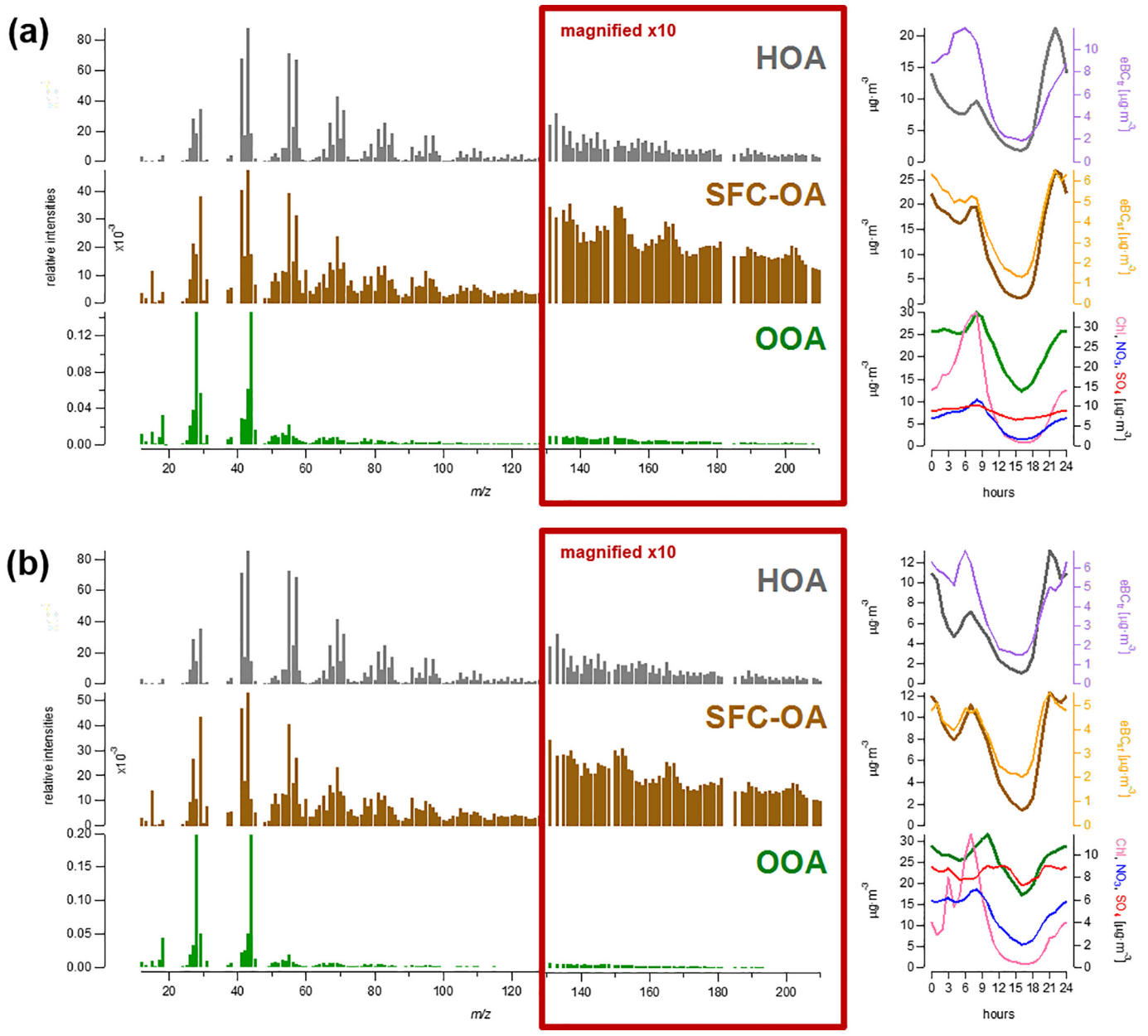

Fig. 4. Average PMF factor mass spectra (left) and diurnal variations of mass concentrations (right) for the fast valve switching setting measurement period (a) 17 February–2 May and (b) 6 May–26 May. Additionally, the diurnal variations of eBC_{tr}, eBC_{sf} (from source apportionment of AE33 data) and chloride are shown with the corresponding ACSM factors.

speed up the oxidation process which makes it harder to separate fresh SFC-OA with unconstrained PMF in April. Therefore, PMF was first performed over the February nights where a relatively high contribution of fresh SFC-OA was observed. The resolved SFC-OA was then used to constrain this factor over the whole period February–April with a random *a*-value of 0.5. Since the switching to the new filament could have influenced the *m/z* 44 contribution, the constrained profile for May allowed a random *a*-value of 1 for *m/z* 44. According to the definition given in Section 2.2.1, the uncertainty of the SFC-OA factor is ±9% for February–April and ±19% for May (Fig. S6), with an average applied *a*-value of 0.24 ± 0.14 and 0.25 ± 0.15, respectively. Fig. S5 shows that the instrument valve switching settings and the instrument tuning had a big impact on the sensitivity towards some PAHs which are expected to be emitted during combustion processes. However, the detailed relationship could not be determined based on our measurements. With the changed sensitivity also the source profile of the SFC-OA changes. With the fast valve switching parameters, the relative intensities of the higher *m/z* (especially above *m/z* 100) as well as their contributions in the SFC-OA increase. PAHs, such as anthracene and pyrene exhibit the same diurnal trend as the SFC-OA factor. Moreover, the correlation of those PAHs over time with the SFC-OA is $R^2 = 0.99$ and $R^2 = 0.95$ for the two periods. The dual-peak diurnal pattern is still very similar to the pattern resolved with the slow valve switching settings. The diurnal correlation with eBC_{sf} is high ($R^2 = 0.97$ and $R^2 = 0.94$, respectively), whereas for the full time series a correlation of $R^2 = 0.76$ and $R^2 = 0.71$ is found, respectively. This is still very high considering that New Delhi has a wide variety of combustion sources. Even in May with an average temperature of 32.2 °C, when residential heating can be excluded, SFC-OA is separated. The more stable combustion sources such as industries (e.g. brick kilns) and especially in April and May, agricultural biomass combustion explain the presence of an SFC-OA factor also in the warmer season. The median ratio of SFC-OA to eBC_{sf} is 2.67 and 1.86, respectively. The change over the measurement campaign is further discussed in Section 3.2.3.

Only one OOA factor was resolved, with an uncertainty of ±11% and ± 4% for the two separate PMF solutions (Fig. S6), respectively.

The chemical fingerprint as well as the diurnal behavior of this factor strongly resemble the MO-OOA 2 from the first measurement period. The mass spectral profile is dominated by *m/z* 44, indicating the oxygenated nature of this factor. This is also reflected in the diurnal pattern, which is more stable compared to the primary sources. Besides contributing substantially to the total OA mass in the afternoon, the characteristic increase of concentration in the late morning hours is also present here. Often, with higher temperatures, one is able to distinguish different OOA factors (Canonaco et al., 2015), however, we are not able to observe this with our data. This may be due to similar dominating precursors in the cold and warm periods in contrast to Europe.

3.2.3. Comparison of the PMF solutions

Even though the source apportionment for this data set was performed on the two valve switching setting measurement periods separately, comparable sources were resolved. For both periods, constraining HOA with the reference spectrum from Crippa et al. (2013b) to separate HOA from other combustion sources was successful. As shown in other studies (Crippa et al., 2014; Elser et al., 2016), this HOA reference profile describes a wide variation of different vehicle fleets and also measurement parameters quite well regarding factor separation in PMF analysis. The diurnal profiles show a similar trend with a smaller rush-hour peak during the morning and high contribution during the evening and the night. The relative contribution to the monthly average is constant from February to May. In December/January, the contribution is lower, probably due to the strong additional source of SFC-OA. The HOA/eBC_{tr} increases from 0.59 to 1.26 from December/January to May. The ratio in December/January is comparable to other ambient studies (Crippa et al., 2013a), whereas the increase of the ratio to even higher values may reflect uncertainties in the determination of eBC_{tr} by the aethalometer model. Uncertainties may come from the assumption used here of overall stable combustion sources represented by a static AAE value. However, further investigation on the BC source apportionment is out of the scope of this paper.

The SFC-OA factor in both periods is characterized by dominant anhydrous sugar fragments at *m/z* 60 and 73. However, the higher *m/z*'s seem to be sensitive to the valve switching settings and/or instrument tuning. Therefore, the SFC-OA profiles are significantly different in the high *m/z* range between the PMF solutions. The fraction of *m/z* 60 decreases slightly over time as it can be expected with increasing temperatures and less residential heating. Estimating the background level of *m/z* 60 was not successful because no period with clear SFC-OA absence could be defined. Other studies defined a background level of 0.3% based on aerosol mass spectrometer (AMS) measurements (Cubison et al., 2011; DeCarlo et al., 2008). Since fragmentation is not entirely consistent across different instruments this value can only serve as a rough guideline. Nevertheless, the stable level of *m/z* 60, clearly above that suggested limit for AMS measurements, also in the warmer season, justifies the constraint of the SFC-OA also in May. Furthermore, PAHs, such as anthracene and pyrene, which are often co-emitted during various combustion processes, show a high correlation with the SFC-OA. Although the sensitivity of the instrument towards the PAHs varies over the campaign, the variance of the PAHs is well explained by the SFC-OA during the nighttime throughout the campaign. The median SFC-OA to eBC_{sf} ratio decreases from 3.30 to 1.86 from December/January to May. Different influences take effect here. Firstly, there is a change in the solid fuel to be expected, because of the high concurrency of very simple local heating (open fires) with solid fuels in the cold period, whereas regional open agricultural burning is more common in the warmer period. In addition, the processing and oxidation process of the SFC-OA will change with the seasons. The f_{60} in the MO-OOA factors in the cold period is on average lower than in the OOA factor in the warmer period, suggesting the SFC-OA is underestimated (Bougiatioti et al., 2014). Furthermore, the BC coating can change due to partitioning, aging or bleaching. Changes in the BC coating and composition will affect the absorption wavelength dependence (Zhang et al., 2018). The data presented here is not able to explain the extent of the influence of the different factors to the change in the SFC-OA/eBC_{sf} values. We were only able to resolve two OOA factors for December/January where MO-OOA 1 exhibits a stronger hydrocarbon pattern than MO-OOA 2. From February to May, PMF is not able to reasonably resolve more than one OOA factor. The highly oxygenated OOA (MO-OOA 2 and OOA, respectively) is very similar for both valve switching settings. These mass spectra are dominated by *m/z* 44. The diurnal profile is more constant compared to the other factors resolved. The morning peak is slightly shifted compared to the primary sources which is likely an indicator of early morning photochemical production of secondary OA.

The absolute concentrations and relative factor contributions to the total OA over the campaign are shown in Fig. 5, and the monthly

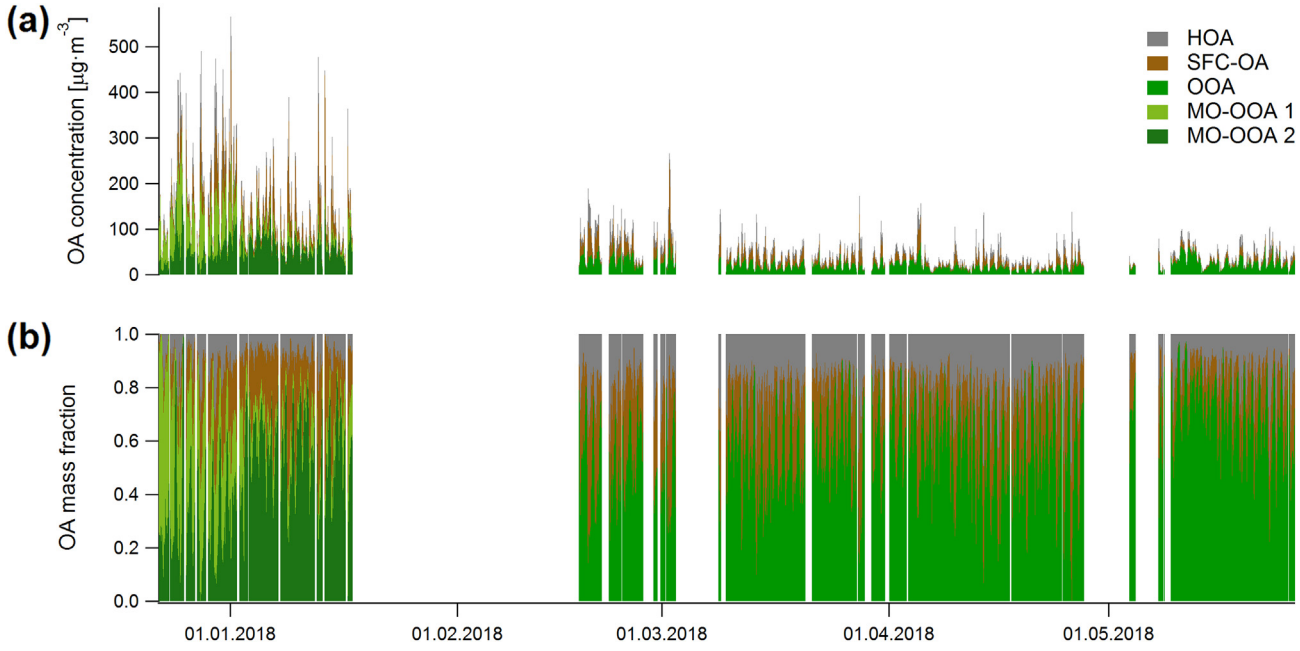

Fig. 5. (a) Absolute and (b) relative factor contributions to the total OA mass.

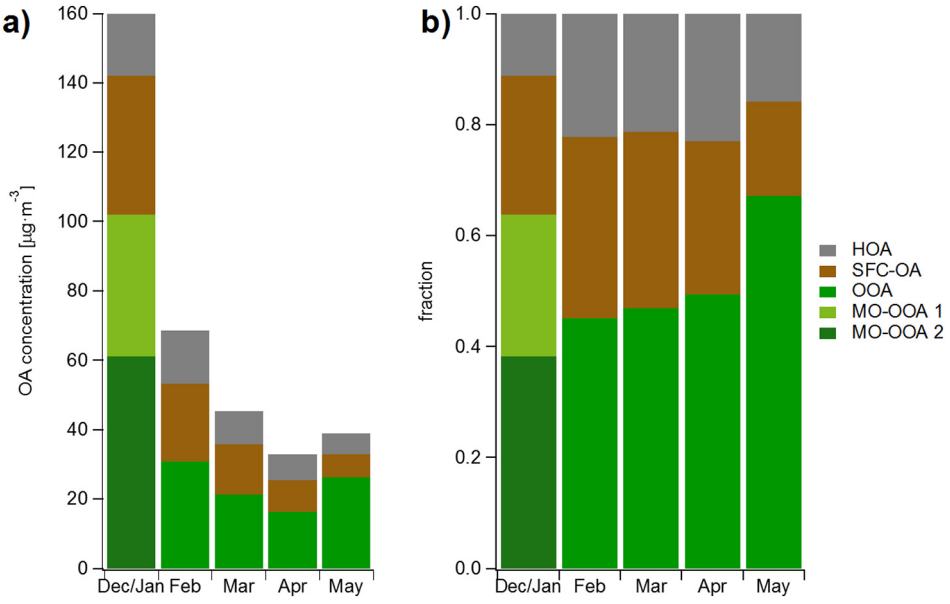

Fig. 6. (a) Monthly averaged total OA composition and (b) relative contributions of the PMF factors to the total OA mass.

averaged OA factors and their contributions to the total OA mass are shown in Fig. 6. Overall, we see that the relative fractions of MO-OOA 2 and OOA are continuously increasing during the campaign, which can be linked to the temperature increase. Over the fast valve switching settings during the campaign, the HOA factor seems to be a stable contributor to the total mass. The SFC-OA contribution at the same time is decreasing. However, even with high temperatures, when it can be assumed that residential heating is minimal, the SFC-OA factor is still present, pointing towards a more stable source of solid fuel combustion. Further studies with higher mass resolution and/or softer ionization could give more insight here.

4. Conclusion

This study investigated the highly time-resolved chemical composition of NR-$PM_{2.5}$ and the source apportionment of OA in New Delhi between December 2017 and May 2018. All species exhibited seasonal as well as diurnal variations. The highest concentrations of all species were observed during the colder period between December and February. With increasing temperatures and greater PBL height, the concentrations decreased. While in the cold period exceptionally high chloride concentrations were measured in the morning hours, the chloride concentration in the warmer period was very low as the equilibrium of ammonium chloride was shifted to the gas phase with the increased temperatures.

The data was recorded in two different valve switching modes. The overall composition and mass loadings of those two modes seemed to be comparable, whereas some ions seemed to behave slightly differently. The different valve switching settings control the amount of time over which material is accumulated and desorbed on the vaporizer and therefore may lead to different mass spectra. Since the ACSM is based on flash vaporization the fast valve switching settings should be preferred. Although PMF was performed separately on the two periods with different valve switching settings, consistent sources were identified for the full period. The primary sources exhibited a stronger diurnal trend compared to the secondary sources, with stronger contribution during nighttime. The MO-OOA 2 (December/January) and OOA (February–May) factors showed high concentrations also during the less polluted afternoon hours. They exhibited an increase in concentration in the late morning when the concentrations of the primary sources were already decreasing. The increase went along with the decrease of the chloride concentration. Further studies focusing on the chemistry in chloride and NO_x rich environments could bring some more insight into the oxidation processes in New Delhi. To better assess the variability of emission sources and the influence of meteorology, rolling PMF, where a small PMF window is shifted over the data set (Canonaco et al., 2020), should be performed over the extended data set. This would also lead to more insight regarding the OOA factors and their evolution over the different seasons.

With this study we are able to give more insight and provide a better understanding of the complex air pollution problem that Delhi is facing. Deconvolving and identifying different sources and their contributions and evolution over time is an important first step to establish better guidelines to reduce air pollution efficiently and to avoid extreme pollution events as observed lately.

CRediT authorship contribution statement

Anna Tobler: Methodology, Software, Validation, Formal analysis, Investigation, Writing - original draft, Writing - review & editing, Visualization. **Deepika Bhattu:** Methodology, Investigation, Writing - review & editing. **Francesco Canonaco:** Software, Formal analysis, Writing - review & editing. **Vipul Lalchandani:** Investigation, Writing - review & editing. **Ashutosh Shukla:** Investigation, Writing - review & editing. **Navaneeth M. Thamban:** Investigation, Writing - review & editing. **Suneeti Mishra:** Investigation, Writing - review & editing. **Atul K. Srivastava:** Resources, Writing - review & editing. **Deewan S. Bisht:** Resources, Writing - review & editing. **Suresh Tiwari:** Resources, Writing - review & editing, Supervision, Project administration, Funding acquisition. **Surender Singh:** Writing - review & editing. **Griša Močnik:** Methodology, Validation, Formal analysis, Writing - review & editing. **Urs Baltensperger:** Writing - review & editing, Supervision. **Sachchida N. Tripathi:** Writing - review & editing, Supervision, Project administration, Funding acquisition. **Jay G. Slowik:** Methodology, Writing - review & editing. **André S.H. Prévôt:** Writing - review & editing, Supervision, Project administration, Funding acquisition.

Declaration of competing interest

F. Canonaco is employed by Datalystica Ltd., the official distributor of the SoFi Pro licenses.

Acknowledgements

This work was financially supported by the Swiss National Science Foundation projects 200021_169787 (SAOPSOAG) and BSSGI0_155846 (IPR-SHOP), the EU Horizon 2020 Framework Programme via the ERA-PLANET project SMURBS (grant agreement no. 689443), the Department of Biotechnology (DBT), Government of India under grant no. BT/IN/UK/APHH/41/KB/2016-17 and the Central Pollution Control Board (CPCB), Government of India under grant no. AQM/Source apportionment EPC Project/2017.

Appendix A. Supplementary data

Supplementary data to this article can be found online at https://doi.org/10.1016/j.scitotenv.2020.140924.

References

Accident Research Cell, Delhi Police, Traffic Police, 2018. Vehicle registration and accident statistics. Road Accidents in Delhi 2018, Toda Pur, New Delhi, p. 110012.

Aerodyne Research Inc, Tofwerk AG, 2019. Time-of-flight Aerosol Chemical Speciation Monitor (ToF-ACSM) User Guide.

Bhandari, S., Gani, S., Patel, K., Wang, D.S., Soni, P., Arub, Z., Habib, G., Apte, J.S., Hildebrandt Ruiz, L., 2019. Sources and atmospheric dynamics of organic aerosol in New Delhi, India: insights from receptor modeling. Atmos. Chem. Phys. 20, 735–752. https://doi.org/10.5194/acp-20-735-2020.

Bougiatioti, A., Stavroulas, I., Kostenidou, E., Zarmpas, P., Theodosi, C., Kouvarakis, G., Canonaco, F., Prevot, A.S.H., Nenes, A., Pandis, S.N., Mihalopoulos, N., 2014. Processing of biomass-burning aerosol in the eastern Mediterranean during summertime. Atmos. Chem. Phys. 14, 4793–4807. https://doi.org/10.5194/acp-14-4793-2014.

Budisulistiorini, S.H., Canagaratna, M.R., Croteau, P.L., Baumann, K., Edgerton, E.S., Kollman, M.S., Ng, N.L., Verma, V., Shaw, S.L., Knipping, E.M., Worsnop, D.R., Jayne, J.T., Weber, R.J., Surratt, J.D., 2014. Intercomparison of an aerosol chemical speciation monitor (ACSM) with ambient fine aerosol measurements in downtown Atlanta, Georgia. Atmos. Meas. Tech. 7, 1929–1941. https://doi.org/10.5194/amt-7-1929-2014.

Canonaco, F., Crippa, M., Slowik, J.G., Baltensperger, U., Prevot, A.S.H., 2013. SoFi, an IGOR-based interface for the efficient use of the generalized multilinear engine (ME-2) for the source apportionment: ME-2 application to aerosol mass spectrometer data. Atmos. Meas. Tech. 6, 3649–3661. https://doi.org/10.5194/amt-6-3649-2013.

Canonaco, F., Slowik, J.G., Baltensperger, U., Prevot, A.S.H., 2015. Seasonal differences in oxygenated organic aerosol composition: implications for emissions sources and factor analysis. Atmos. Chem. Phys. 15, 6993–7002. https://doi.org/10.5194/acp-15-6993-2015.

Canonaco, F., Tobler, A., Chen, G., Sosedova, Y., Slowik, J.G., Bozzetti, C., Daellenbach, K.R., El Haddad, I., Crippa, M., Huang, R.J., Furger, M., Baltensperger, U., Prevot, A.S.H., 2020. A new method for long-term source apportionment with time-dependent factor profiles and uncertainty assessment using SoFi Pro: application to one year of organic aerosol data. Atmos. Meas. Tech. Discuss. https://doi.org/10.5194/amt-2020-204.

CCFA, 2019. The French Automotive Industry: Analysis & Statistics 2018, Paris.

Chirico, R., DeCarlo, P.F., Heringa, M.F., Tritscher, T., Richter, R., Prévôt, A.S.H., Dommen, J., Weingartner, E., Wehrle, G., Gysel, M., Laborde, M., Baltensperger, U., 2010. Impact of aftertreatment devices on primary emissions and secondary organic aerosol formation potential from in-use diesel vehicles: results from smog chamber experiments. Atmos. Chem. Phys. 10, 11545–11563. https://doi.org/10.5194/acp-10-11545-2010.

Chirico, R., Prevot, A.S.H., DeCarlo, P.F., Heringa, M.F., Richter, R., Weingartner, E., Baltensperger, U., 2011. Aerosol and trace gas vehicle emission factors measured in a tunnel using an aerosol mass spectrometer and other on-line instrumentation. Atmos. Environ. 45, 2182–2192. https://doi.org/10.1016/j.atmosenv.2011.01.069.

Crenn, V., Sciare, J., Croteau, P.L., Verlhac, S., Fröhlich, R., Belis, C.A., Aas, W., Auml;ijala, M., Alastuey, A., Artinano, B., Baisnee, D., Bonnaire, N., Bressi, M., Canagaratna, M., Canonaco, F., Carbone, C., Cavalli, F., Coz, E., Cubison, M.J., Esser-Gietl, J.K., Green, D.C., Gros, V., Heikkinen, L., Herrmann, H., Lunder, C., Minguillon, M.C., Mocnik, G., O'Dowd, C.D., Ovadnevaite, J., Petit, J.E., Petralia, E., Poulain, L., Priestman, M., Riffault, V., Ripoll, A., Sarda-Esteve, R., Slowik, J.G., Setyan, A., Wiedensohler, A., Baltensperger, U., Prevot, A.S.H., Jayne, J.T., Favez, O., 2015. ACTRIS ACSM intercomparison - part 1: reproducibility of concentration and fragment results from 13 individual quadrupole aerosol chemical speciation monitors (Q-ACSM) and consistency with co-located instruments. Atmos. Meas. Tech. 8, 5063–5087. https://doi.org/10.5194/amt-8-5063-2015.

Crippa, M., DeCarlo, P.F., Slowik, J.G., Mohr, C., Heringa, M.F., Chirico, R., Poulain, L., Freutel, F., Sciare, J., Cozic, J., Di Marco, C.F., Elsasser, M., Nicolas, J.B., Marchand, N., Abidi, E., Wiedensohler, A., Drewnick, F., Schneider, J., Borrmann, S., Nemitz, E., Zimmermann, R., Jaffrezo, J.L., Prevot, A.S.H., Baltensperger, U., 2013a. Wintertime aerosol chemical composition and source apportionment of the organic fraction in the metropolitan area of Paris. Atmos. Chem. Phys. 13, 961–981. https://doi.org/10.5194/acp-13-961-2013.

Crippa, M., El Haddad, I., Slowik, J.G., DeCarlo, P.F., Mohr, C., Heringa, M.F., Chirico, R., Marchand, N., Sciare, J., Baltensperger, U., Prevot, A.S.H., 2013b. Identification of marine and continental aerosol sources in Paris using high resolution aerosol mass spectrometry. J. Geophys. Res.-Atmos. 118, 1950–1963. https://doi.org/10.1002/jgrd.50151.

Crippa, M., Canonaco, F., Lanz, V.A., Aijala, M., Allan, J.D., Carbone, S., Capes, G., Ceburnis, D., Dall'Osto, M., Day, D.A., DeCarlo, P.F., Ehn, M., Eriksson, A., Freney, E., Hildebrandt Ruiz, L., Hillamo, R., Jimenez, J.L., Junninen, H., Kiendler-Scharr, A., Kortelainen, A.M., Kulmala, M., Laaksonen, A., Mensah, A., Mohr, C., Nemitz, E., O'Dowd, C., Ovadnevaite, J., Pandis, S.N., Petaja, T., Poulain, L., Saarikoski, S., Sellegri, K., Swietlicki, E., Tiitta, P., Worsnop, D.R., Baltensperger, U., Prevot, A.S.H., 2014. Organic aerosol components derived from 25 AMS data sets across Europe using a consistent ME-2 based source apportionment approach. Atmos. Chem. Phys. 14, 6159–6176. https://doi.org/10.5194/acp-14-6159-2014.

Cubison, M.J., Ortega, A.M., Hayes, P.L., Farmer, D.K., Day, D., Lechner, M.J., Brune, W.H., Apel, E., Diskin, G.S., Fisher, J.A., Fuelberg, H.E., Hecobian, A., Knapp, D.J., Mikoviny, T., Riemer, D., Sachse, G.W., Sessions, W., Weber, R.J., Weinheimer, A.J., Wisthaler, A., Jimenez, J.L., 2011. Effects of aging on organic aerosol from open biomass burning smoke in aircraft and laboratory studies. Atmos. Chem. Phys. 11, 12049–12064. https://doi.org/10.5194/acp-11-12049-2011.

Dall'Osto, M., Ovadnevaite, J., Ceburnis, D., Martin, D., Healy, R.M., O'Connor, I.P., Kourtchev, I., Sodeau, J.R., Wenger, J.C., O'Dowd, C., 2013. Characterization of urban aerosol in Cork city (Ireland) using aerosol mass spectrometry. Atmos. Chem. Phys. 13, 4997–5015. https://doi.org/10.5194/acp-13-4997-2013.

Davison, A.C., Hinkley, D.V., 1997. Bootstrap Methods and Their Application. Cambridge University Press.

DeCarlo, P.F., Dunlea, E.J., Kimmel, J.R., Aiken, A.C., Sueper, D., Crounse, J., Wennberg, P.O., Emmons, L., Shinozuka, Y., Clarke, A., Zhou, J., Tomlinson, J., Collins, D.R., Knapp, D., Weinheimer, A.J., Montzka, D.D., Campos, T., Jimenez, J.L., 2008. Fast airborne aerosol size and chemistry measurements above Mexico City and Central Mexico during the MILAGRO campaign. Atmos. Chem. Phys. 8, 4027–4048. https://doi.org/10.5194/acp-8-4027-2008.

Drinovec, L., Mocnik, G., Zotter, P., Prevot, A.S.H., Ruckstuhl, C., Coz, E., Rupakheti, M., Sciare, J., Muller, T., Wiedensohler, A., Hansen, A.D.A., 2015. The "dual-spot" aethalometer: an improved measurement of aerosol black carbon with real-time loading compensation. Atmos. Meas. Tech. 8, 1965–1979. https://doi.org/10.5194/amt-8-1965-2015.

Drinovec, L., Gregorič, A., Zotter, P., Wolf, R., Bruns, E.A., Prévôt, A.S.H., Petit, J.E., Favez, O., Sciare, J., Arnold, I.J., Chakrabarty, R.K., Moosmüller, H., Filep, A., Močnik, G., 2017. The filter-loading effect by ambient aerosols in filter absorption photometers depends on the coating of the sampled particles. Atmos. Meas. Tech. 10, 1043–1059. https://doi.org/10.5194/amt-10-1043-2017.

Elser, M., Huang, R.J., Wolf, R., Slowik, J.G., Wang, Q.Y., Canonaco, F., Li, G.H., Bozzetti, C., Daellenbach, K.R., Huang, Y., Zhang, R.J., Li, Z.Q., Cao, J.J., Baltensperger, U., El-Haddad, I., Prevot, A.S.H., 2016. New insights into PM2.5 chemical composition and sources in two major cities in China during extreme haze events using aerosol mass spectrometry. Atmos. Chem. Phys. 16, 3207–3225. https://doi.org/10.5194/acp-16-3207-2016.

European Commission, 2018. Statistical Pocketbook 2018: EU Transport in Figures. https://doi.org/10.2832/05477.

Favez, O., El Haddad, I., Piot, C., Boréave, A., Abidi, E., Marchand, N., Jaffrezo, J.L., Besombes, J.L., Personnaz, M.B., Sciare, J., Wortham, H., George, C., D'Anna, B., 2010. Inter-comparison of source apportionment models for the estimation of wood burning aerosols during wintertime in an Alpine city (Grenoble, France). Atmos. Chem. Phys. 10, 5295–5314. https://doi.org/10.5194/acp-10-5295-2010.

Fire Information for Resource Management System: https://firms.modaps.eosdis.nasa.gov/map, access: 18.11.2019, 2019.

Freney, E., Zhang, Y.J., Croteau, P., Amodeo, T., Williams, L., Truong, F., Petit, J.E., Sciare, J., Sarda-Esteve, R., Bonnaire, N., Arumae, T., Aurela, M., Bougiatioti, A., Mihalopoulos, N., Coz, E., Artinano, B., Crenn, V., Elste, T., Heikkinen, L., Poulain, L., Wiedensohler, A., Herrmann, H., Priestman, M., Alastuey, A., Stavroulas, I., Tobler, A., Vasilescu, J., Zanca, N., Canagaratna, M., Carbone, C., Flentje, H., Green, D., Maasikmets, M., Marmureanu, L., Minguillon, M.C., Prevot, A.S.H., Gros, V., Jayne, J., Favez, O., 2019. The second ACTRIS inter-comparison (2016) for aerosol chemical speciation monitors (ACSM): calibration protocols and instrument performance evaluations. Aerosol Sci. Technol. https://doi.org/10.1080/02786826.2019.1608901.

Fröhlich, R., Cubison, M.J., Slowik, J.G., Bukowiecki, N., Prevot, A.S.H., Baltensperger, U., Schneider, J., Kimmel, J.R., Gonin, M., Rohner, U., Worsnop, D.R., Jayne, J.T., 2013. The ToF-ACSM: a portable aerosol chemical speciation monitor with TOFMS detection. Atmos. Meas. Tech. 6, 3225–3241. https://doi.org/10.5194/amt-6-3225-2013.

Fröhlich, R., Crenn, V., Setyan, A., Belis, C.A., Canonaco, F., Favez, O., Riffault, V., Slowik, J.G., Aas, W., Aijala, M., Alastuey, A., Artinano, B., Bonnaire, N., Bozzetti, C., Bressi, M., Carbone, C., Coz, E., Croteau, P.L., Cubison, M.J., Esser-Gietl, J.K., Green, D.C., Gros, V., Heikkinen, L., Herrmann, H., Jayne, J.T., Lunder, C.R., Minguillon, M.C., Mocnik, G., O'Dowd, C.D., Ovadnevaite, J., Petralia, E., Poulain, L., Priestman, M., Ripoll, A., Sarda-Esteve, R., Wiedensohler, A., Baltensperger, U., Sciare, J., Prevot, A.S.H., 2015a. ACTRIS ACSM intercomparison - part 2: intercomparison of ME-2 organic source apportionment results from 15 individual, co-located aerosol mass spectrometers. Atmos. Meas. Tech. 8, 2555–2576. https://doi.org/10.5194/amt-8-2555-2015.

Fröhlich, R., Cubison, M.J., Slowik, J.G., Bukowiecki, N., Canonaco, F., Croteau, P.L., Gysel, M., Henne, S., Herrmann, E., Jayne, J.T., Steinbacher, M., Worsnop, D.R., Baltensperger, U., Prévôt, A.S.H., 2015b. Fourteen months of on-line measurements of the non-refractory submicron aerosol at the Jungfraujoch (3580 m a.s.l.) – chemical composition, origins and organic aerosol sources. Atmos. Chem. Phys. 15, 11373–11398. https://doi.org/10.5194/acp-15-11373-2015.

Fuzzi, S., Baltensperger, U., Carslaw, K., Decesari, S., van Der Gon, H.D., Facchini, M.C., Fowler, D., Koren, I., Langford, B., Lohmann, U., Nemitz, E., Pandis, S., Riipinen, I., Rudich, Y., Schaap, M., Slowik, J.G., Spracklen, D.V., Vignati, E., Wild, M., Williams, M., Gilardoni, S., 2015. Particulate matter, air quality and climate: lessons learned

and future needs. Atmos. Chem. Phys. 15, 8217–8299. https://doi.org/10.5194/acp-15-8217-2015.

Gani, S., Bhandari, S., Seraj, S., Wang, D.S., Patel, K., Soni, P., Arub, Z., Habib, G., Hildebrandt Ruiz, L., Apte, J., 2019. Submicron aerosol composition in the world's most polluted megacity: the Delhi aerosol supersite study. Atmos. Chem. Phys. 19, 6843–6859. https://doi.org/10.5194/acp-19-6843-2019.

Goel, R., Mohan, D., Guttikunda, S.K., Tiwari, G., 2016. Assessment of motor vehicle use characteristics in three Indian cities. Transp. Res. Part D: Transp. Environ. 44, 254–265. https://doi.org/10.1016/j.trd.2015.05.006.

Grieshop, A.P., Logue, J.M., Donahue, N.M., Robinson, A.L., 2009. Laboratory investigation of photochemical oxidation of organic aerosol from wood fires 1: measurement and simulation of organic aerosol evolution. Atmos. Chem. Phys. 9, 1263–1277. https://doi.org/10.5194/acp-9-1263-2009.

IEA, 2016. Energy and Air Pollution. World Energy Outlook Special Report. OECD/IEA, Paris.

Kumar, S., Aggarwal, S.G., Sarangi, B., Malherbe, J., Barre, J.P.G., Berail, S., Seby, F., Donard, O.F.X., 2018. Understanding the influence of open-waste burning on urban aerosols using metal tracers and lead isotopic composition. Aerosol Air Qual. Res. 18, 2433–2446. https://doi.org/10.4209/aaqr.2017.11.0510.

Lalchandani, V., Kumar, V., Tobler, A., Navaneeth, M. T., Mishra, S., Slowik, J. G., Bhattu, D., Rai, P., Rangu, S., Ganguly, D., Tiwari, S., Ragosti, N., Tiwari, S., Mocnik, G., Prévôt, A. S. H., and Tripathi, S. N.: Real-time characterization and source apportionment of fine particulate matter in the Delhi megacity area during late winter, submitted to Sci. Total Environ., 2020.

Liu, T., Marlier, M.E., DeFries, R.S., Westervelt, D.M., Xia, K.R., Fiore, A.M., Mickley, L.J., Cusworth, D.H., Milly, G., 2018. Seasonal impact of regional outdoor biomass burning on air pollution in three Indian cities: Delhi, Bengaluru, and Pune. Atmos. Environ. 172, 83–92. https://doi.org/10.1016/j.atmosenv.2017.10.024.

Middlebrook, A.M., Bahreini, R., Jimenez, J.L., Canagaratna, M.R., 2012. Evaluation of composition-dependent collection efficiencies for the aerodyne aerosol mass spectrometer using field data. Aerosol Sci. Technol. 46, 258–271. https://doi.org/10.1080/02786826.2011.620041.

Nagpure, A.S., Ramaswami, A., Russell, A., 2015. Characterizing the spatial and temporal patterns of open burning of municipal solid waste (MSW) in Indian cities. Environ. Sci. Technol. 49, 12904–12912. https://doi.org/10.1021/acs.est.5b03243.

Ng, N.L., Canagaratna, M.R., Zhang, Q., Jimenez, J.L., Tian, J., Ulbrich, I.M., Kroll, J.H., Docherty, K.S., Chhabra, P.S., Bahreini, R., Murphy, S.M., Seinfeld, J.H., Hildebrandt, L., Donahue, N.M., DeCarlo, P.F., Lanz, V.A., Prévôt, A.S.H., Dinar, E., Rudich, Y., Worsnop, D.R., 2010. Organic aerosol components observed in northern hemispheric datasets from aerosol mass spectrometry. Atmos. Chem. Phys. 10, 4625–4641. https://doi.org/10.5194/acp-10-4625-2010.

Ng, N.L., Herndon, S.C., Trimborn, A., Canagaratna, M.R., Croteau, P.L., Onasch, T.B., Sueper, D., Worsnop, D.R., Zhang, Q., Sun, Y.L., Jayne, J.T., 2011. An aerosol chemical speciation monitor (ACSM) for routine monitoring of the composition and mass concentrations of ambient aerosol. Aerosol Sci. Technol. 45, 780–794. https://doi.org/10.1080/02786826.2011.560211.

Paatero, P., 1997. Least squares formulation of robust non-negative factor analysis. Chemometr. Intell. Lab. 37, 23–35. https://doi.org/10.1016/S0169-7439(96)00044-5.

Paatero, P., 1999. The multilinear engine - a table-driven, least squares program for solving multilinear problems, including the n-way parallel factor analysis model. J. Comput. Graph. Stat. 8, 854–888. https://doi.org/10.2307/1390831.

Paatero, P., Tapper, U., 1994. Positive matrix factorization - a nonnegative factor model with optimal utilization of error-estimates of data values. Environmetrics 5, 111–126. https://doi.org/10.1002/env.3170050203.

Pant, P., Baker, S.J., Goel, R., Guttikunda, S., Goel, A., Shukla, A., Harrison, R.M., 2016. Analysis of size-segregated winter season aerosol data from New Delhi, India. Atmos. Pollut. Res. 7, 100–109. https://doi.org/10.1016/j.apr.2015.08.001.

Petit, J.E., Favez, O., Sciare, J., Crenn, V., Sarda-Esteve, R., Bonnaire, N., Mocnik, G., Dupont, J.C., Haeffelin, M., Leoz-Garziandia, E., 2015. Two years of near real-time chemical composition of submicron aerosols in the region of Paris using an aerosol chemical speciation monitor (ACSM) and a multi-wavelength aethalometer. Atmos. Chem. Phys. 15, 2985–3005. https://doi.org/10.5194/acp-15-2985-2015.

Pieber, S.M., El Haddad, I., Slowik, J.G., Canagaratna, M.R., Jayne, J.T., Platt, S.M., Bozzetti, C., Daellenbach, K.R., Fröhlich, R., Vlachou, A., Klein, F., Dommen, J., Miljevic, B., Jimenez, J.L., Worsnop, D.R., Baltensperger, U., Prevot, A.S.H., 2016. Inorganic salt interference on CO2+ in aerodyne AMS and ACSM organic aerosol composition studies. Environ. Sci. Technol. 50, 10494–10503. https://doi.org/10.1021/acs.est.6b01035.

Pope, C.A., Dockery, D.W., 2006. Health effects of fine particulate air pollution: lines that connect. J. Air Waste Manage. Assoc. 56, 709–742. https://doi.org/10.1080/10473289.2006.10464485.

Ravindra, K., Wauters, E., Tyagi, S.K., Mor, S., Van Grieken, R., 2006. Assessment of air quality after the implementation of compressed natural gas (CNG) as fuel in public transport in Delhi, India. Environ. Monit. Assess. 115, 405–417. https://doi.org/10.1007/s10661-006-7051-5.

Sandradewi, J., Prevot, A.S.H., Szidat, S., Perron, N., Alfarra, M.R., Lanz, V.A., Weingartner, E., Baltensperger, U., 2008. Using aerosol light absorption measurements for the quantitative determination of wood burning and traffic emission contributions to particulate matter. Environ. Sci. Technol. 42, 3316–3323. https://doi.org/10.1021/es702253m.

Singh, A.K., 2013. In: Hdqrs, D. (Ed.), Office of the Deputy Commissioner of Police: Traffic. Delhi Gazette.

Tiwari, S., Chate, D.M., Pragya, P., Ali, K., Bisht, D.S., 2012. Variations in mass of the PM10, PM2.5 and PM1 during the monsoon and the winter at New Delhi. Aerosol Air Qual. Res. 12, 20–29. https://doi.org/10.4209/aaqr.2011.06.0075.

Tiwari, S., Srivastava, A.K., Bisht, D.S., Parmita, P., Srivastava, M.K., Attri, S.D., 2013. Diurnal and seasonal variations of black carbon and PM2.5 over New Delhi, India: influence of meteorology. Atmos. Res. 125-126, 50–62. https://doi.org/10.1016/j.atmosres.2013.01.011.

Wang, L., Slowik, J.G., Tripathi, N., Bhattu, D., Rai, P., Kumar, V., Vats, P., Satish, R., Baltensperger, U., Ganguly, D., Rastogi, N., Sahu, L.K., Tripathi, S.N., Prévôt, A.S.H., 2020. Source characterization of volatile organic compounds measured by PTR-ToF-MS in Delhi, India. Atmos. Chem. Phys. Discuss https://doi.org/10.5194/acp-2020-11.

WHO, 2005. WHO Air Quality Guidelines for Particulate Matter, Ozone, Nitrogen Dioxide and Sulfur Dioxide - Global Update 2005. World Health Organization.

Xu, W., Croteau, P., Williams, L., Canagaratna, M., Onasch, T., Cross, E., Zhang, X., Robinson, W., Worsnop, D., Jayne, J., 2017. Laboratory characterization of an aerosol chemical speciation monitor with PM2.5 measurement capability. Aerosol Sci. Technol. 51, 69–83. https://doi.org/10.1080/02786826.2016.1241859.

Zhang, Y., Favez, O., Canonaco, F., Liu, D., Močnik, G., Amodeo, T., Sciare, J., Prévôt, A.S.H., Gros, V., Albinet, A., 2018. Evidence of major secondary organic aerosol contribution to lensing effect black carbon absorption enhancement. Npj Clim. Atmos. Sci. 1, 47. https://doi.org/10.1038/s41612-018-0056-2.

Zhao, R., Lee, A.K.Y., Huang, L., Li, X., Yang, F., Abbatt, J.P.D., 2015. Photochemical processing of aqueous atmospheric brown carbon. Atmos. Chem. Phys. 15, 6087–6100. https://doi.org/10.5194/acp-15-6087-2015.

Zhou, W., Gao, M., He, Y., Wang, Q., Xie, C., Xu, W., Zhao, J., Du, W., Qiu, Y., Lei, L., Fu, P., Wang, Z., Worsnop, D.R., Zhang, Q., Sun, Y., 2019. Response of aerosol chemistry to clean air action in Beijing, China: insights from two-year ACSM measurements and model simulations. Environ. Pollut. 255, 113345. https://doi.org/10.1016/j.envpol.2019.113345.

Zotter, P., Herich, H., Gysel, M., El-Haddad, I., Zhang, Y.L., Mocnik, G., Huglin, C., Baltensperger, U., Szidat, S., Prevot, A.H., 2017. Evaluation of the absorption Ångström exponents for traffic and wood burning in the aethalometer-based source apportionment using radiocarbon measurements of ambient aerosol. Atmos. Chem. Phys. 17, 4229–4249. https://doi.org/10.5194/acp-17-4229-2017.